LBNL-44341

ERNEST ORLANDO LAWRENCE
BERKELEY NATIONAL LABORATORY

Investigating Ion-Surface Collisions with a Niobium Superconducting Tunnel Junction Detector in a Time-of-Flight Mass Spectrometer

G. Westmacott, F. Zhong, M. Frank, S. Friedrich,
S. Labov, and W.H. Benner

Engineering Division

December 1999

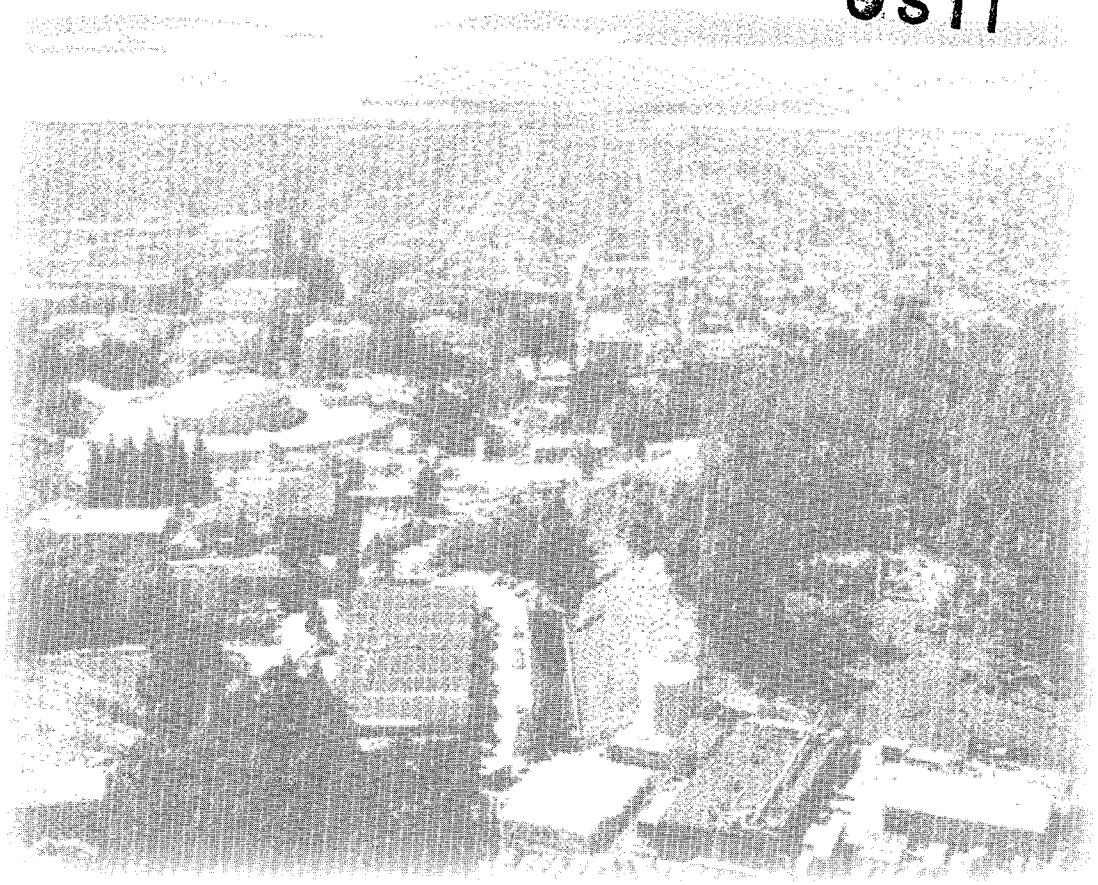

DISCLAIMER

Portions of this document may be illegible in electronic image products. Images are produced from the best available original document.

LBNL-44341

Investigating Ion-Surface Collisions with a Niobium Superconducting Tunnel Junction Detector in a Time-of-Flight Mass Spectrometer

G. Westmacott,[1] F. Zhong,[1] M. Frank,[2] S. Friedrich,[2]
S. Labov,[2] and W.H. Benner[1]

[1]Engineering Division
Ernest Orlando Lawrence Berkeley National Laboratory
University of California
Berkeley, California 94720

[2]Lawrence Livermore National Laboratory
7000 East Avenue, L-418
Livermore, California 94551

December 1999

This work was supported by the Director, Office of Science, Office of Biological and Environmental Research under U.S. Department of Energy Contract No. DE-AC03-76SF00098 and also performed under the auspices of the U.S. Department of Energy by LLNL under Contract No. W-7405-ENG-48. We would also like to thank Professor Werner Ens from the Department of Physics at the University of Manitoba for some helpful and stimulating discussions.

Investigating Ion-surface Collisions with a Niobium Superconducting Tunnel Junction Detector in a Time-of-flight Mass Spectrometer

G. Westmacott[1], F. Zhong[1], M. Frank[2], S. Friedrich[2], S. Labov[2] and W.H. Benner[1]*
[1]Lawrence Berkeley National Laboratory, MS 70A-3363, 1 Cyclotron Road, Berkeley, CA 94720
[2]Lawrence Livermore National Laboratory, 7000 East Ave., L-418 Livermore, CA 94551

Abstract
The performance of an energy sensitive, niobium superconducting tunnel junction detector is investigated by measuring the pulse height produced by impacting molecular and atomic ions at different kinetic energies. Ions are produced by laser desorption and matrix-assisted laser desorption in a time-of-flight mass spectrometer. Our results show that the STJ detector pulse height decreases for increasing molecular ion mass, passes through a minimum at around 2000 Da, and the increases with increasing mass of molecular ions above 2000Da.* The detector does not show a decline in sensitivity for high mass ions as is observed with microchannel plate ion detectors.* These detector plus height measurements are discussed in terms of several physical mechanisms involved in an ion-surface collision.

Introduction
Detection of ions in time-of-flight mass spectrometry (TOF-MS) is typically accomplished by an ion-surface collision, in which the secondary electrons emitted in the collision are used to generate a measurable signal. Microchannel plates (MCPs), electron multipliers, and conversion dynodes are examples of ion detectors that rely on ion-surface collisions and the formation of secondary electrons to generate an output signal. For these types of detectors, the probability of producing secondary electrons in an ion-surface collision directly relates to how efficiently ions can be detected. Thus, ion detection becomes difficult when the probability of secondary electron formation is small.

It is well established that the secondary electron yield decreases with decreasing velocity of the molecular ion.[1-4] As a result, the probability of producing secondary electrons is small for large, slow moving molecular ions. For example, a 66-kDa ion at 26 keV has a probability less than 0.2 of producing secondary electrons.[3] This decrease in the efficiency of producing secondary electrons limits the performance of mass spectrometry as an analytical tool.

In contrast to secondary electron emission, measurements of secondary *ion* emission indicate that the efficiency is close to 100% and does not appear to decrease significantly, if at all, with increasing primary ion mass.[2,5,6] Other types of detectors have also been developed with the goal of overcoming the limitations with detectors that rely on secondary electron emission. For example, there are ion-to-photon,[7] inductive,[8] and charge[9, 10] detectors.

Since the secondary electron yield is dependent on the incident velocity of the primary molecular ion, and thus its kinetic energy, secondary electron detectors can also be used to resolve incident ions with different kinetic energies. In particular, this idea has been used to distinguish between ions of different charge states.[11-13] This technique was named by the Uppsala group secondary electron resolved mass spectrometry (SERMS). [11] This method of

resolving the kinetic energy (and thus, charge state) of ions, with its dependence on the production of secondary electrons, has limitations for low velocity, high mass molecular ions. In addition to SERMS, passivated solid state detectors are also energy sensitive. However, they have a much higher energy threshold, measuring ions with kinetic energies around 500 keV,[14] which precludes their use in a typical mass spectrometer.

Cryogenic detectors, such as superconducting tunnel junction (STJ) detectors[15, 16] or hot-electron microcalorimeters,[17] are also energy sensitive, and thus can measure the energy deposited by incident ions. In contrast to SERMS, cryogenic detectors do not rely on the emission of secondary electrons to produce a signal. For cryogenic detectors, as long as the deposited energy is greater than the thermal energy and electronic noise, there should not be high mass detection limitations as there are for secondary electron detectors. See review articles by D. Twerenbold[18] and N. Booth *et al.*[19] for more details about cryogenic detectors in general, and M. Frank, *et al.*[20] for a discussion on their application to TOF-MS. Cryogenic detectors, being energy sensitive, offer a unique tool for investigating certain fundamental aspects of mass spectrometry, for example, the nature of the ion-surface collisions.

In this paper, we describe our investigation of the performance of a niobium STJ detector by measuring the pulse height produced with several types of molecular and atomic ions at different kinetic energies. There have been extensive investigations into the use of STJ detectors with x-ray detection; however, to date, there has been very little systematic work on characterizing its response for ion detection. We also attempt to interpret our measurements by discussing several physical mechanisms involved in an ion-surface collision.

Experimental

Mass Spectrometry Setup

A schematic diagram of the experimental setup is shown in Fig. 1. Measurements were made using a linear time-of-flight mass spectrometer with a matrix-assisted laser desorption/ionization (MALDI) ion source and a STJ detector, which is mounted inside a pumped helium cryostat. A N_2 laser (VSL-337ND: Laser Science, Inc., Cambridge, MA, USA) is operated at ~10 Hz and focused onto a rotatable MALDI sample stage. Positive ions formed from a laser pulse are accelerated and focused by the concave shape of the sample stage (shown in Fig. 2) onto the STJ detector. Focusing the ion beam onto the relatively small surface of the STJ helps increase the ion count rate compared to the count rate for a standard flat sample stage. Though focusing the ion beam is not necessary for detecting ions with the STJ, it does decrease the amount of time required to achieve appropriate statistics.

The concave sample stage shown in Fig. 2 creates an ion beam focal length that depends on the voltage difference between the sample stage and the first grid. The concave shape introduces the need to align critically the laser beam with the center of the concave sample stage; otherwise, the beam is deflected off center. The optimum voltage ratio for the sample stage to the first grid is about 3:2, producing an ion beam focus near the surface of the STJ. This was first determined using the SIMION program, and subsequently verified using a MCP-phosphorus screen detector to observe the beam profile. Deflection plates were also used for fine adjustment of the radial position of the ion beam focus.

The accelerating voltage, V_a, was varied between 10 kV and 30 kV for all samples. In the interest of starting with less complicated projectiles, atomic ions and small clusters were analyzed before large biomolecular ions were studied. The first sample was CsI and was

prepared by dissolving it in water and depositing enough on the surface to form, when dried, a thin white layer of CsI crystals. The second sample, prepared similarly, consisted of roughly a 1:1:1:1 molar mixture of CsI, RbCl, KCl and NaCl. Finally, the third sample was prepared using standard methods in MALDI, with sinapinc acid as the matrix, and a mixture of insulin (5733 Da) and myoglobin (16900 Da).

Superconducting Tunnel Junction (STJ) Detector Basics

STJ detectors typically consist of two layers of superconductors separated by a thin insulating barrier. For the detector used in this experiment, the top layer is a 100-nm thick niobium film, the middle is a ~2-nm aluminum oxide tunneling barrier, and the bottom layer is a 260-nm thick niobium film on a silicon substrate. The size of the active area of the STJ detector is 0.04 mm^2.

The STJ detector is held in good thermal contact with the pumped liquid ^{4}He bath inside a cryostat. The outer dimensions of the cryostat are 40 cm in height by 19 cm in diameter. A liquid N_2 bath (77 K) in the top chamber in the cryostat, shown in Fig. 1, helps reduce the boil-off of liquid ^{4}He in the lower bath. By pumping directly on the liquid ^{4}He bath with a mechanical pump, the temperature is reduced from 4.2 K at atmospheric pressure to an operating temperature of T = 1.3 K. As illustrated in Fig. 1, there is a series of small metal apertures inside the cryostat, aligned with the MALDI sample stage and the STJ detector, which reduce the amount of thermal radiation reaching the surface of the STJ detector.

STJ detectors operate best at a temperature T well below the critical temperature T_c of the superconducting films, typically with $T \approx 0.1T_c$. At this low temperature, nearly all the conduction electrons of the superconducting layers have formed weakly bound pairs, called Cooper pairs. The binding energy of the Cooper pairs is 2Δ, where Δ is the superconducting energy gap, typically on the order of 1 meV; for Nb, Δ = 1.55 mV. Operating STJ detectors at a temperature well below T_c minimizes the thermal breakage of Cooper pairs. For Nb, T_c = 9.2 K. In this experiment the detector was operated at a temperature of 1.3 K.

When an ion strikes the STJ detector, phonons (lattice vibrations) are created with some energy distribution. Phonons with energy greater than 2Δ can break Cooper pairs, creating excess quasiparticles (electron and hole-like excitations) in a superconductor that can tunnel through the insulating barrier. By applying an appropriate bias voltage (typically around a few hundred μV) across the STJ detector, tunneling of the excess quasiparticles through the insulating barrier results in a measurable current pulse. This current pulse decays with a time constant given by the quasiparticle lifetime. The magnitude of the current pulse is proportional to the number of quasiparticles that tunnel, which is proportional to the number of phonons created by the impacting ion.

During operation, a small magnetic field (~100 Gauss) must be applied parallel to the plane of the junction in order to suppress the dc Josephson effect. That is, the magnetic field suppresses Cooper pair tunneling, which otherwise results in a large background current (supercurrent) and additional noise. A small background current (on the order of tens of micro-amps) remains despite the magnetic field because of tunneling quasiparticles from thermally broken Cooper pairs. A typical characteristic I (V) curve, with an applied magnetic field of ~100 Gauss, is shown in Fig. 3A. The bias voltage for the STJ was set such that the signal-to-noise was maximum. Typically, this occurs on the plateau of the I(V) curve around ~500 μV. Maximizing the signal-to-noise was accomplished using the signal generated with x-rays from

an ^{55}Fe source that can be temporarily mounted in front of our STJ detector (not shown in Fig. 1).

Signal Processing

A custom built pre-amplifier supplies the voltage bias to the junction and amplifies the tunnel-current pulses. A schematic of this current-sensitive pre-amplifier is shown in Fig. 3B. It employs a dc voltage for stable biasing in regions of high dynamic resistance, and a FET input stage for low-noise pulse amplification. For more details see S. Friedrich, *et al.*.[21]

The pre-amplifier signal is digitized with a LeCroy 7200 oscilloscope. Fig. 4 shows the signal (part of the oscilloscope trace) from the impact of a *single* 30 keV molecular ion of insulin. For every laser shot, the trace from the oscilloscope was transferred and stored by a computer for off-line analysis. Each trace contained from zero to 20 ion pulses. Using custom software, a table of flight times and pulse-heights is generated from the digitized record for every laser shot. This allows the generation of both a complete TOF spectrum *and*, for an individual ion species, a detector pulse-height (energy) spectrum. The flight time of an ion is taken to be the *start* of the STJ detector pulse (as indicated in Fig. 4), and the pulse height is measured from baseline before the onset of the pulse.

Results and Discussion

The rise time of a pulse from the STJ detector (as shown in Fig. 4) is around 500 ns, and thus, along with the signal-to-noise, imposes a limitation on time resolution. With such detector pulses, ion arrival times could be measured with about ±50 ns precision. However, this is not the main limiting factor for the analysis of large, slow moving molecular ions, where the velocity (and, consequently time) spread of the ions limits the resolution.

With off-line analysis of the STJ detector pulses (like the typical pulse shown in Fig. 4), scatter plots of pulse-height versus ion flight time can be generated for MALDI samples. Such a scatter plot is shown in Fig. 5 for a mixture of insulin and myoglobin in sinapinic acid matrix with accelerating voltage V_a = 30 kV. The corresponding time-of-flight spectrum is shown in the lower part of Fig. 5 with *Counts* (the number of ion detection events) plotted on the *y*-axis. Each point in the scatter plot corresponds to a STJ detector pulse resulting from a detection event involving one or more ions. Vertical clusters of data points correspond to specific ions, and coincide with the peaks in the TOF spectrum. For a given vertical cluster of data points (that is, a specific m/z range), a histogram of the STJ detector pulse height can be generated.

STJ Pulse-height (Energy) Spectra

A pulse-height histogram (spectrum) were generated for each ion species in this experiment, and are shown for three ion species in Fig. 6. The top pulse-height spectrum is for Cs+ ions with V_a = 30 kV (scatter plot is not shown), and the bottom two graphs are pulse-height spectra for insulin and myoglobin from the scatter plot shown in Fig. 5. In each pulse-height spectrum, the predominant peak at low pulse-height (<60 mV) corresponds to detection events where exactly one, singly charged ion collided with the detector. The next smaller peak at approximately twice the pulse-height gives the number of detection events involving two ions that impact in coincidence. Finally, at approximately three times the average single-ion pulse-height in Fig. 6, there are a small number of detection events with three ions impacting in coincidence.

Two (or more) ions are said to impact in "coincidence" when they impact with the surface of the STJ detector within less than ~500 ns (the rise time of the detector pulse) of each other. As a result of two ions arriving in coincidence, the STJ detector generates a pulse that is approximately twice as high as a pulse from a single ion (because the two ions have twice the kinetic energy as a single ion). If two ions arrive at times with a difference greater than 500 ns, the pulse from the first ion will be decaying by the time the second ion impacts, thus, two separated pulses (detection events) will be resolved and counted. However, pulses that start on the tail of a previous pulse are discarded because the determination of the pulse-height is difficult. This "pile-up" rejection is done by the custom software mentioned above.

For molecular ions, the peak in pulse-height spectra at twice the average single-ion pulse-height could correspond to one doubly charged dimer, as suggested by Bae, *et al.*.[14] However, in our experiment the contribution from $2M^{2+}$ must be small. This can be determined by observing that, in Fig. 6, the ratio of single-ion to 2-ion detection events for the Cs^+ (where dimer formation of Cs is unlikely) is the same as for the molecular ions. In addition, Fig. 5 shows a relatively small number of $2M^+$ for both insulin and myoglobin.

The peaks in the pulse-height spectra shown in Fig. 6 (for insulin and myoglobin) can be seen in the form of horizontal bands in the scatter plot shown in Fig. 5. The lower, darker band corresponds to the predominate peak in the pulse-height spectra at low pulse height, and thus are detection events involving only one ion. A second band lies above the dark band. It is less dense and mostly corresponds to detection events involving two ions.

In Fig. 6, the pulse height for two ions arriving in coincidence is slightly less than twice the pulse height for a single ion, even though two ions have twice the kinetic energy as a single ion. This difference could be explained by a small nonlinear response of the STJ detector, which is currently under investigation. This small difference in pulse height may also be a result of simply adding two analog pulses, which occur at slightly different times (less than 500 ns). The amplitude resulting when two pulses do not coincide exactly will be less than the sum of the amplitudes for the individual pulses, which are separated by a small time.

Pulse-height (energy) resolution of the STJ detector

As observed from the pulse-height spectra in Fig. 6, the pulse-height (energy) resolution for atomic species is about nine for atomic species. For example, 30 keV Cs^+ ions generate a peak (as shown in Fig. 6) with a FWHM that corresponds to about 3.3 keV. The *time resolution* for Cs^+ implies that the ions have a kinetic energy spread on the order of a few hundred electronvolts which certainly cannot account for the 3.3 keV energy spread measured by the STJ detector. For our detection setup, using the same method of pulse-height analysis as with the signal from ions, the energy resolution for x-rays from a ^{55}Fe radioactive source (data not shown) is the same as that for atomic ions.

The energy resolution is about a factor of two smaller for larger molecular ions like insulin and myoglobin than atomic species. For example, the measured deposited energy spread for insulin at 30 keV is about 6.5 keV, a factor of two larger than for Cs^+. This factor of two is may be attributed to the many different channels through which energy can be lost by large, more structurally complicated ions. The various mechanisms of energy loss experienced by a molecular ion are discussed below. A low-energy tail on the peaks for insulin and, especially for myoglobin (see Fig. 6) also contributes to the width of the molecular ion peaks in the pulse-height spectra. This is most likely a result of in-flight fragmentation of the ions with one or more of the fragments missing the detector. For example, if a 30 keV molecular ion fragments

in half and only one half collides with the STJ detector, then only half the energy (pulse-height) will be measured compared to the intact molecular ion. The peak distribution may also be skewed to lower energies by ions hitting near the edge of the STJ detector, and, consequently, more phonons may escape out the edges of the detector and not create any quasiparticles.

With detector pulse-height (energy) resolution between 4 and 9 for the STJ detector used in this experiment, it is easy to distinguish different ion charge states, such as singly-charged ions from doubly-charged ion. Charge discrimination with cryogenic detectors has been demonstrated previously.[15, 16] Other methods for separating charge states using secondary electron emission, [11-13] have much lower resolution, as well as limitations imposed by decreasing electron emission efficiency for detecting larger molecular ions. Though separating ion charge states can be useful, the STJ detector can more finely resolve differences in measured energy, for example, in the deposited energy for different ion species with the same kinetic energy. This is discussed in the next two sections.

Deposited Energy as a Function of Species

As shown in Fig. 6, an interesting aspect of the pulse-height spectra is that the average pulse amplitude is slightly different for each ion species, even though they each have approximately the same kinetic energy. A similar trend can also be observed in the data shown by G. Hilton, *et al.*[17] using a cryogenic microcalorimeter which measures the total thermal energy deposited by a particle impact.

To further investigate these differences in the STJ detector pulse height for different ion species, the STJ detector pulse heights were measured for impacting CsI clusters, $(CsI)_nCs^+$, as well as alkali atomic ions. The results, plotted as a function of kinetic energy, are shown in Fig. 7. In Fig. 7A, larger molecular clusters of CsI, with the same average kinetic energy, give detector pulses with *smaller* amplitude. For example, the STJ pulse height is about 20% larger for Cs^+ than for $(CsI)Cs^+$, with the STJ detector measuring about 5 keV more energy for Cs^+. In contrast, for the atomic ion data shown in Fig. 7B, the STJ detector cannot resolve differences in the deposited energy for different atomic ions with the same average kinetic energy. These results suggest that the energy transferred to the surface of the STJ is more strongly dependent on the *number* of atomic constituents than the molecular mass.

A similar plot to that shown in Fig.7 for atomic and cluster ions is shown for insulin and myoglobin in Fig. 8. At the same average kinetic energy, the detector pulse from impacting myoglobin (16900 Da) has a larger amplitude than that from insulin (5734 Da), an opposite trend to that observed for the low mass the CsI clusters.

Another way of plotting this data is shown in Fig. 9 where the STJ detector pulse height is plotted as a function of mass for two different accelerating voltages. The line through the data is simply a guide for the eye. At low mass, the amplitude of the STJ detector pulse rapidly decreases with increasing mass, passes through a minimum near 2000 Da, and increases again as the mass of the ions rises above 2000 Da. There is about an 8 keV energy difference between the energy measured at mass 2000 Da and the energy measured for the larger masses. (The 8 keV was calculated by dividing 12 mV, which is the approximate difference between the minimum pulse-height at 2000 Da and a larger pulse-heights at high mass, by 45 mV, which is approximately the average pulse-pulse height for 30 keV ions, and multiplying by 30 keV.) This minimum in STJ pulse amplitude is also evident in bands in the scatter plot shown in Fig. 5. The same curves in Fig. 9 also fit the horizontal bands in Fig. 5.

Interpretation of STJ Detector Pulse Height Measurements

The graphs in Figs. 7 and 8 show that the amplitude of the STJ detector pulses is proportional to the impinging ion's kinetic energy. Extrapolating the lines back to zero detector-amplitude leads to a x-intercept at about 3 ± 1 keV. This intercept represents the practical lower energy detection threshold for the STJ detectors used in this experiment. STJ detector signals below this become lost in the noise of the preamplifier. Practically, however, the counting rate and signal-to-noise ratio became too low to acquire acceptable statistics for ions with kinetic energy less than 10 keV.

The STJ detector pulse height is likely to depend on several factors. The most obvious factors contributing to the STJ detector pulse height are the kinetic energy and internal energy of the incident ion, where internal energy of the ion is mainly due to the many vibrational and rotational energy states for large molecular ions. The effect of having larger internal ion energy is that the STJ detector pulse height would increase, and thus the lines shown in Figs. 7 and 8 would be shifted up. Since the data fits well to a straight line down to an ion kinetic energy of 10 keV, the internal energy has to be much less than 10 keV, which is not surprising. We estimate that for biomolecules with mass on the order of tens of kilo-Daltons, and temperature around 400-500 K, [22] that the internal energy is less than 1 keV.

Energy-loss mechanisms that compete for the total energy (kinetic and internal energy) of the impinging ion are processes such as the breaking of bonds, plastic deformation of surface, surface sputtering, recoiling fragments from the impacting ion, and phonons that escape to the edges of the STJ detector without not creating any quasiparticles. A rough estimate (order of magnitude) for the energy carried away by sputtered material, can be calculated by noting that sputter yields are around 50 for 8 keV argon incident on frozen glycerol, [23,24] and that, in general, axial energies for secondary ions are up to 2 eV (independent of the incident mass and velocity).[25] Thus for atomic projectiles, on the order of 100 eV could be carried away by sputtered material. For small incident keV cluster of Cs^+, up to [2(CsI)]Cs+, ion yields of Au^- are at most a factor of 10 higher than for atomic species.[26] Assuming that the total sputter yields are also a factor of 10 higher, then on the order of kilo-electron-volts of energy can be carried way from the surface by sputtered material. The energy difference between the energy carried away by sputtered material from an atomic and molecular collisions is consistent with the difference in STJ detector pulse height shown in Fig. 7 for atomic and CsI clusters. However, there is about 10 keV more energy measured by the STJ detector for Cs^+ than there is for $(CsI)_2Cs^+$, and the energy carried away by sputtered material does not likely account for this entire difference. The above estimates are an oversimplification, and, for example, do not take into account that for every sputtered particle, a bond was broken.

The above estimates may account for the observed decrease in pulse height for increasing masses below 2000 Da (Fig 9). The increase in the STJ detector pulse height for masses above 2000 Da could partly be a result of an increase in internal energy for larger molecular ions. However, it is unlikely that the molecular ion internal energy could account for the entire 8 keV difference between the pulse-height minimum at 2000 Da and the energy measured for larger molecular ions. Estimates for how the total energy of large molecular ions is distributed between the many processes involved (sputtering, bond breaking, and phonon creation) in a collision with the STJ surface is beyond the scope of this paper.

The phonon spectrum generated by an ion colliding with a surface may also affect the response of the STJ detector because phonons are measured only when their energy is above 2Δ, the binding energy of the Coopers pairs. The phonon spatial and energy distribution may

depend on the total energy deposited by the impacting ion by affecting the temperature and size of the local hot spot created. It may also depend on impact velocity. If the velocity of the ion is greater than the speed of sound in the surface of the detector, a shock wave is created and would likely affect the phonon spectrum.

In general, the curvature of the data in Fig. 9 suggests that there are at least two mechanisms competing for the total energy of the incident ion molecular ion. For example, it seems that there is a "molecular coupling effect" that becomes dominant above some critical mass (~2000 Da) or number of atomic constituents. Below this critical ion mass (size), energy loss due to sputtering and bond breaking may be dominant. For certain, the minimum of STJ detector pulse height for ion masses around 2000 Da is caused by having fewer high energy phonons generated in an ion-surface collision.

There may be a small amount of ice and other frozen material on the detector surface because of the low temperature of the STJ (1.3 K). This, in effect, would decrease the energy transferred to the top Nb because a fraction of the phonons could be absorbed by the ice or reflected back into the ice layer at the ice-Nb boundary. Under normal operation throughout a day of measurements, degradation of the detector's response was not observed. A decrease in STJ detector pulse height can be observed after briefly exposing the cooled STJ detector to air, however.

Ion energy measurements have also been made by the NIST group using a microcalorimeter cryogenic detector[17] where they calibrated their detector using x-rays from a ^{55}Fe radioactive source mounted near the detector. As mentioned in the experimental section, a ^{55}Fe source is mounted in front of our STJ detector, however it was only used as a diagnostic tool and to generate detection events while optimizing the settings, for example, the appropriate bias voltage. In our experiment with an STJ detector, we did not calibrate the energy (pulse-height) measurements with a x-ray source because the mechanism for transferring energy to a surface is different for ions and photons. There is no obvious relationship between the energy measured for x-rays and the energy measured for ions.

Future work

In general, for the STJ detector, the small size and operation at low temperatures limits its practicality for routine ion detection in mass spectrometry. However, these limitations will likely soon be reduced with the development of cryogenic detector arrays and closed-cycle coolers. Still, with the current configuration and with no loss in sensitivity for large mass detection, the STJ detector may be well suited for quantitative analysis. For example, the STJ detector could be used to analyze high mass polymer distributions, or measuring ionization efficiencies of the MALDI process.

Further experiments are clearly necessary to understand better the differences observed in the STJ detector response to molecular ions of different masses. Future experiments will entail varying the detector material (and thus changing phonon energy threshold to break quasiparticles), and using other types of cryogenic detectors, like a microcalorimeter detector. Also, to try and investigate the internal energy of MALDI ions, the impacting kinetic energy could be reduced by post-deceleration, keeping the MALDI sample stage voltage constant at 30 kV. By doing this, the count rate would not suffer as it does when the accelerating voltage is reduced, and thus better ion counting statistics could be achieved. Finally, if the ion beam could be aligned to hit the STJ detector, it may be useful to use it in a reflecting-TOF instrument to remove contributions from fragment ions.

Conclusions

A superconducting tunnel junction detector has been operated in a MALDI TOF MS to investigate its performance. The STJ detector pulse height for various molecular and atomic ions at different kinetic energies was investigated. We expect, based on its operating principle, that the STJ detector is 100% efficient. Our results are consistent with this expectation, showing that the STJ detector pulse height increases with increasing mass of molecular ions above about 2000 Da rather than decreasing if the detector was not 100% efficient. For an ion colliding with the detector with sufficient energy (greater than ~5 keV for the STJ detector used in this experiment), a measurable signal will always be produced, regardless of its mass. This is a unique feature which can be used to investigate fundamental aspects of mass spectrometry, or used for quantitative characterization of other processes, for example measuring ionization efficiencies for the MALDI process.

The STJ detector offers a unique way to study ion-surface collisions of low energy (keV) ions. Experiments that investigate ion-surface collision commonly measure yields and energy distributions of particles ejected from a surface. The STJ detector allows observation of other process that take place *in* the surface, that is, the creation of phonons. To better understand the differences in the STJ detector pulse height (response) for various molecular and atomic ions, further experiments are necessary. In the interest of better understanding ion-surface collisions, the goal is to try to correlate the STJ detector pulse height (that is, the energy deposited in the surface that creates phonons) with other processes, such as sputtering, that compete for the total energy of the ion. We have speculated on this correlation and will continue to investigate the energetics of ion-surface collisions using the STJ detector.

Acknowledgments

We would like to thank Professor Werner Ens from the Department of Physics at the University of Manitoba for some helpful and stimulating discussions. This work was supported by the Director, Office of Energy Research, Office of Health and Environmental Research, Human Genome Program, U.S. Department of Energy under contract number DE-AC03-76SF00098, and also performed under the auspices of the U.S. Department of Energy by LLNL under contract number W-7405-ENG-48.

References

1. P.W. Geno and R.D. Macfarlane, *Int. J. Mass Spectrom. Ion Process.* 92, 195 (1989).
2. G. Westmacott, W. Ens and K.G. Standing, *Nucl. Instr. and Meth.* B 108, 282 (1996).
3. A. Brunelle, P. Chaurand, S. Della-Negra, Y. Le Beyec and E. Parillis, *Rapid Commun. Mass Spectrom.* 11, 353 (1997).
4. G. Westmacott, M. Frank, S.E. Labov, and W.H. Benner, in preparation for *Rapid Commun. Mass Spectrom.*
5. A. Brunelle, P. Chaurand, S. Della-Negra, Y. Le Beyec and G.B. Baptista, *Int. J. Mass Spectrom. Ion Process.* 126, 65 (1993).
6. V. Nguyen, K. Wien, I.V. Baranov, A.C. Novikov, and V.V. Obnorskii, Rapid Commun. Mass Spectrom. 10, 1463 (1996)
7. F. Dubois, R. Knochenmuss, and Zenobi, *Int. J. Mass Spectrom. Ion Process.* 169/170, 89 (1997)
8. M.A. Park, J.H. Callahan, *Rapid Commun. Mass Spectrom.* 8, 317 (1994)
9. S. D. Fuerstenau and W.H. Benner, *Rapid Commun. Mass Spectrom.* 9, 1528 (1995)
10. U. Bahr, U. Röhling, C. Lautz, K. Strupat, M. Schürenberg, F. Hillenkamp, *Int. J. Mass Spectrom. Ion Process.* 153, 9 (1996)
11. J. Axelson, C.T. Reimann, and B.U.R. Sundqvist, *Int. J. Mass Spectrom. Ion Process.* 133, 141 (1994).
12. P.V. Bondarenko, P.G. Grant, and R.D. Macfarlane, *Int. J. Mass Spectrom. Ion Process.* 133, 181 (1994).
13. I. Chernushevich, W. Ens, and K.G. Standing, in "Electrospray Ionization Mass Spectrometry", ed. R.B. Cole, John Wiley & Sons, 1997.
14. Y.K. Bae, R.J. Beuhler, Y.Y. Chu, G. Friedlander, Y. Xu, and L. Friedman, *Nucl. Instrum. and Meth.* B 114, 185 (1996).
15. W.H. Benner, A.T. Barfknecht, M. Frank, D.M. Horn, J.M. Jaklevic, S. Labov and C. Mears, *J. Am. Soc. Mass Spectrom.* 8, 1094 (1997).
16. M. Frank, A.T. Barfknecht, W.H. Benner, D.M. Horn, J.M. Jaklevic, S. Labov and C. Mears, *Rapid Commun. Mass Spectrum.* 10, 1946 (1996).
17. G.C. Hilton, J.M. Martinis, D.A. Wollman, K.D. Irwin, L.L. Dulcie, D. Gerber, P.M. Gillevet, and D. Twerenbold, *Nature* 391, 672 (1998).
18. D. Twerenbold, *Report on Progress in Particle Physics* 59, 349 (1996)
19. N.E. Booth, B. Cabrera, and E. Fiorini, *Ann. Rev. of Nuc. and Part. Sci.* 49, 471 (1996)
20. M. Frank, S.E. Labov, G. Westmacott, W.H. Benner, to be published in *Mass Spectrom. Rev.* (1999).
21. S. Friedrich, K. Segall, M.C. Gaidis, C.M. Wilson, D.E. Prober, P.J. Kindlman, A.E. Szymkowiak, and S.H. Moseley, *IEEE Trans. Appl. Supercon.* **7**, 3383 (1997)
22. C.D. Nowry, M.V. Johnston, *J. Phys. Chem.* 98, 1904 (1994).
23. P. Williams and G. Gillen, in *Ion Formation from Organic Solids IFOS IV*, ed. A. Benninghoven, Wiley, Chichester, p. 15 (1898).
24. G. Gillen, J.W. Christiansen, I.S. Tsong, B. Kimball, and P. Williams, *Rapid Commun. Mass Spectrom.* 2, 67 (1988).
25. W. Ens, in *Fundamental Processes in Sputtering of Atoms and Molecules (SPUT92)*, ed. P. Sigmund, Munksgaard, Copenhagen, p. 155 (1993); and references therein.

26. M.G. Blain, S. Della-Negra, H. Joret, Y. LeBeyec, and E.A. Schweikert, J. Vac. Sci. Technol. A 8, 2265 (1990).

Figure Captions

Fig. 1: Schematic diagram of experimental setup, which is not drawn to scale.

Fig. 2: Schematic diagram of the rotatable, concaved MALDI sample-stage, which focuses the ions on to the surface of the STJ detector.

Fig. 3: (A) Characteristic I-V curve of the Nb STJ when operated at 1.3 K and with a magnetic field (~100 Gauss) applied parallel to the surface of the STJ to suppress the supercurrent caused by Cooper pair tunneling (the dc Josephson effect). Typical operating voltage bias is ~500 μV. (B) Schematic of the current-sensitive preamplifier for the STJ detector.

Fig. 4: A sample STJ detector pulse for one impacting insulin ion at 30 keV. For two insulin ions colliding in coincidence, the detector pulse would have about twice the amplitude.

Fig. 5: The top graph is a typical scatter plot of the raw data from the STJ detector. Every point corresponds to an ion impact event. The corresponding time-of-flight spectrum is shown below. The *y*-axis, *Counts*, is the number of detector pulses counted per time bin. Scatter plots were typically generated from about 5000 laser shots. This relatively large number of laser shots was necessary to achieve reasonable statistics and compensated for the small size of the STJ detector.

Fig. 6: STJ pulse-height (energy) spectra for various ions. All ions are accelerated to 30 keV and thus have approximately the same average kinetic energy. Note the shift in the average STJ pulse height for the different species as indicated by the arrows.

Fig. 7: STJ detector pulse height plotted as a function of primary ion kinetic energy. (A) Small molecular clusters of $(CsI)_nCs^+$ and atomic Cs^+. (B) Atomic ions only.

Fig. 8: STJ detector pulse height plotted as a function of primary ion kinetic energy for large molecular ions.

Fig. 9: STJ detector pulse height plotted as a function of primary ion mass using two different accelerating voltage.

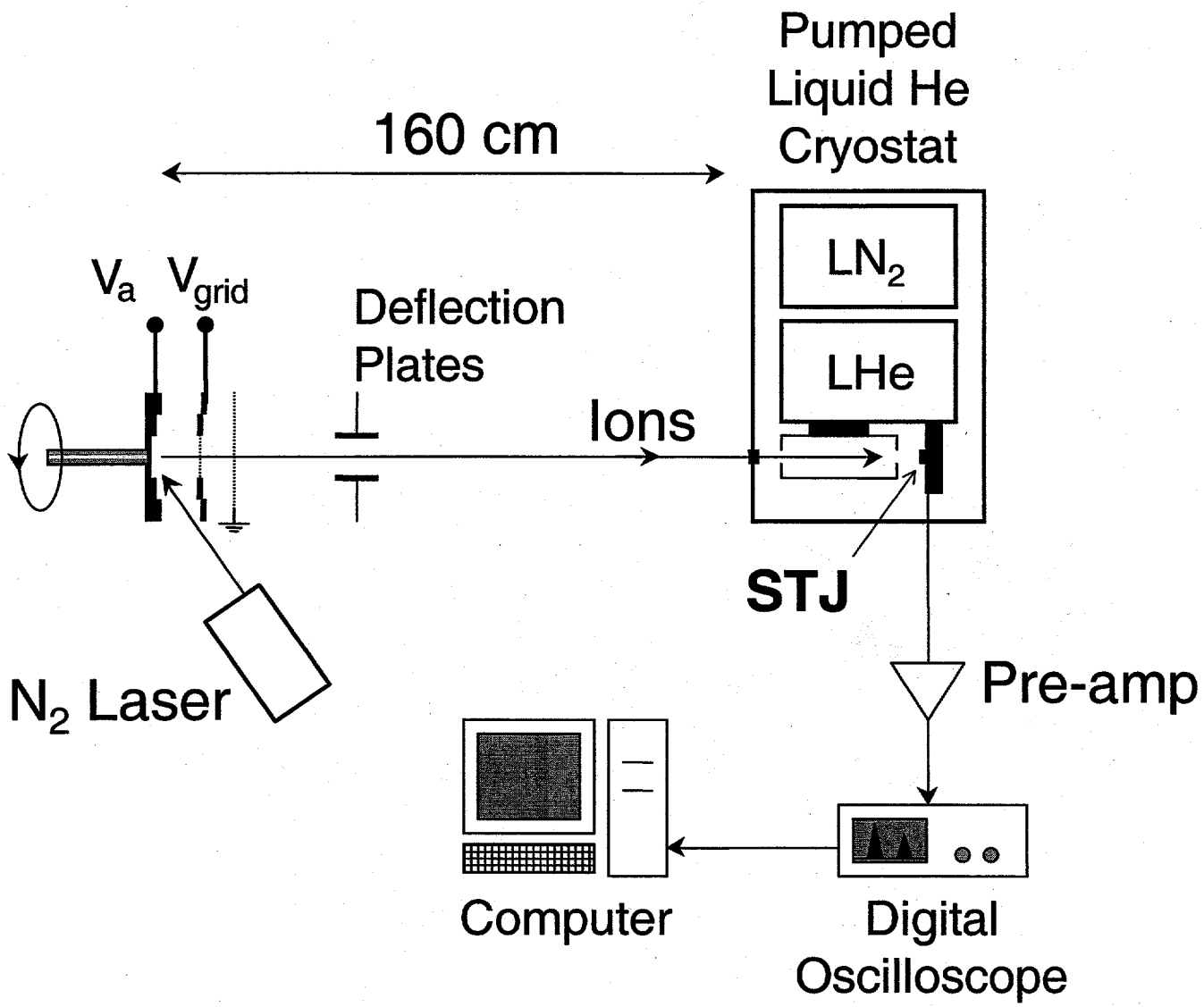
Pumped
Liquid He
Cryostat
160 cm
V_a V_{grid}
Deflection
Plates
LN_2
LHe
Ions
STJ
N_2 Laser
Pre-amp
Computer
Digital
Oscilloscope

Fig.1

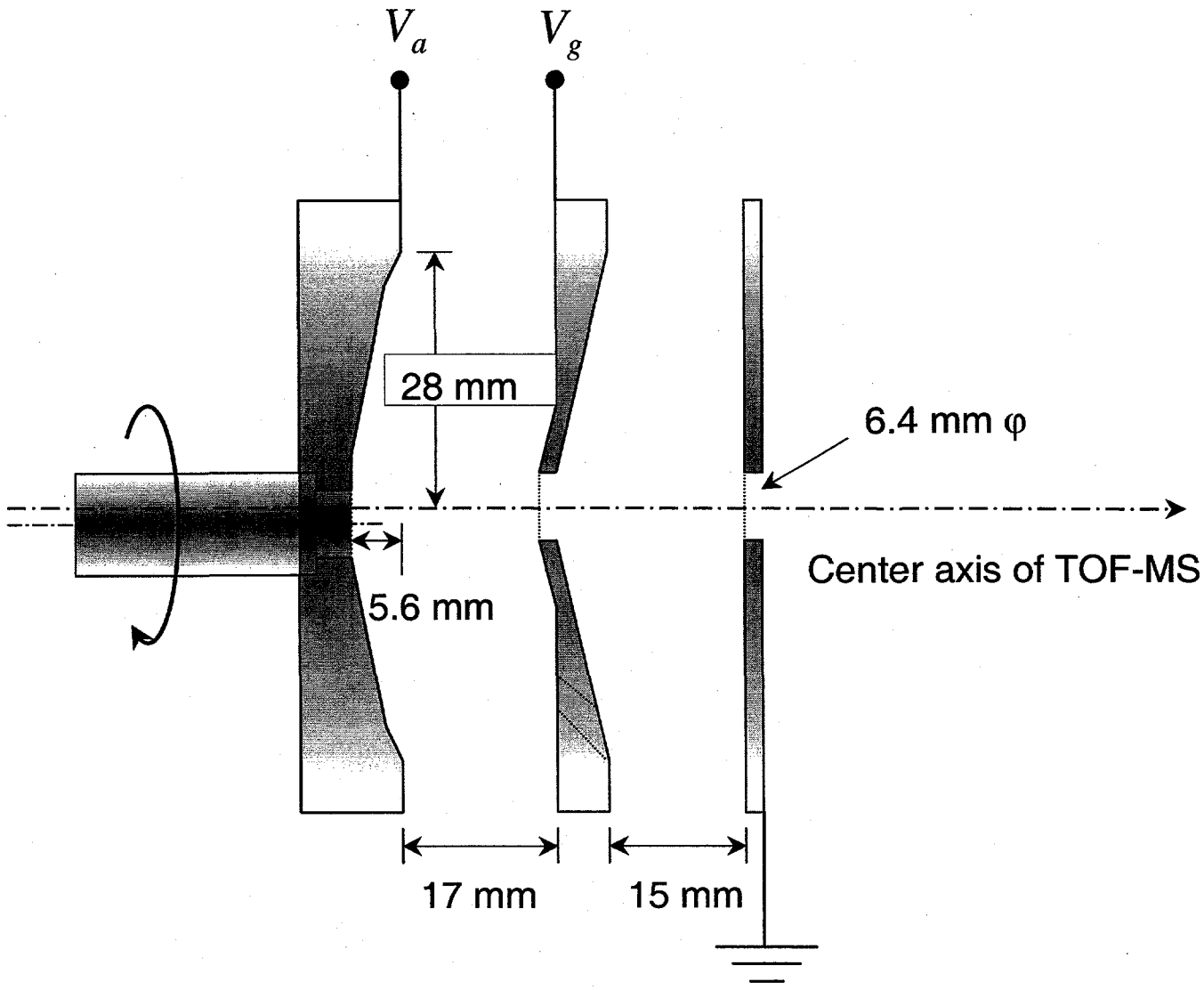

Fig.2

(A)

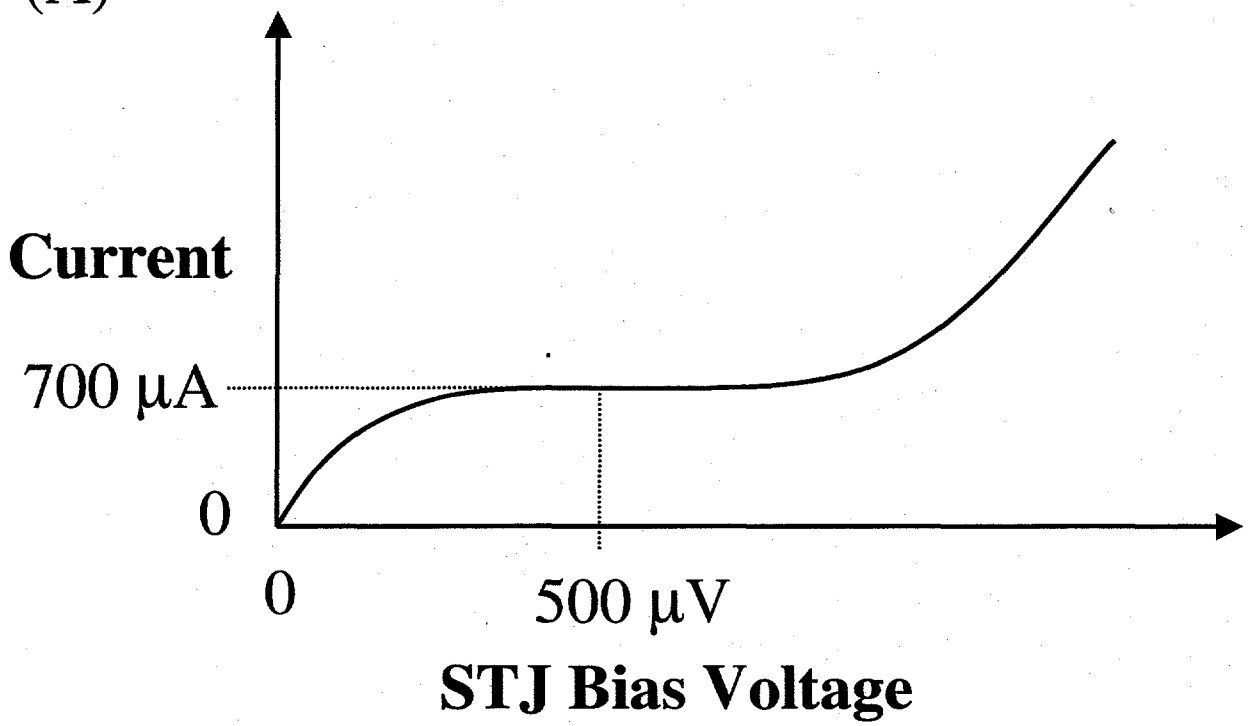
Current
700 μA
0
0
500 μV
STJ Bias Voltage

(B)

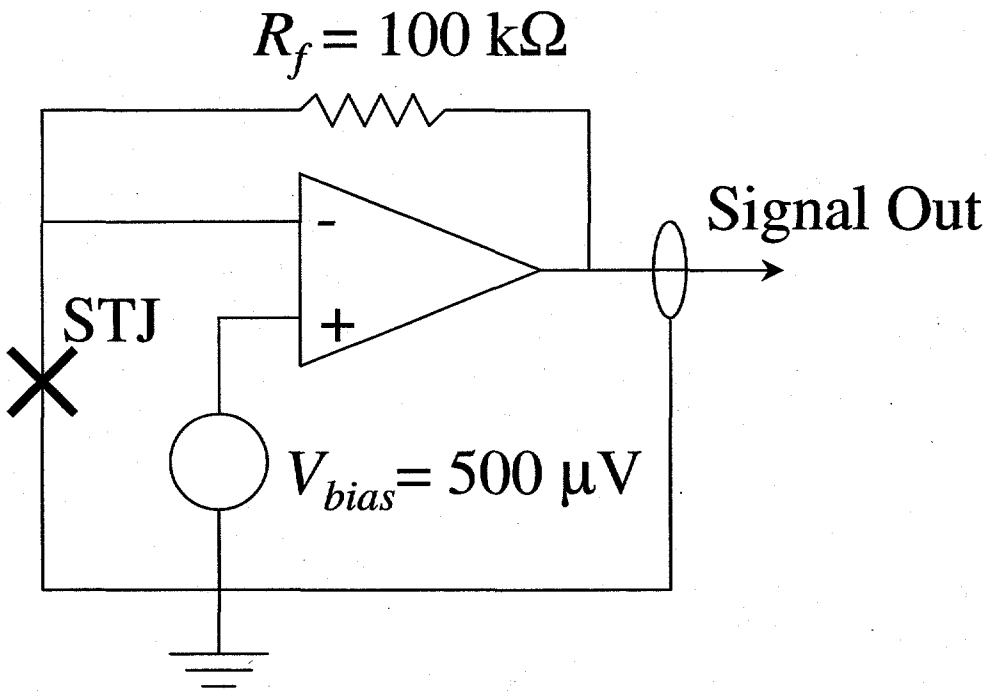
R_f = 100 kΩ
-
+
Signal Out
STJ
V_{bias}= 500 μV

Fig.3

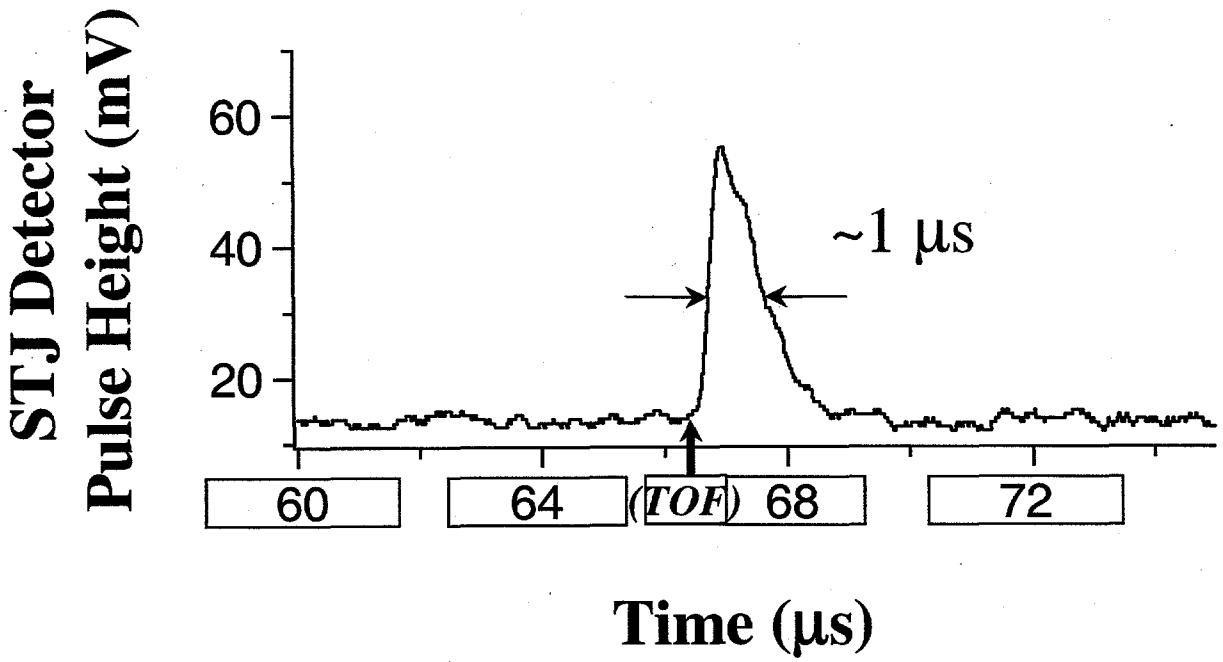
STJ Detector
Pulse Height (mV)
60
40
20
~1 μs
60
64
(TOF)
68
72
Time (μs)

Fig.4

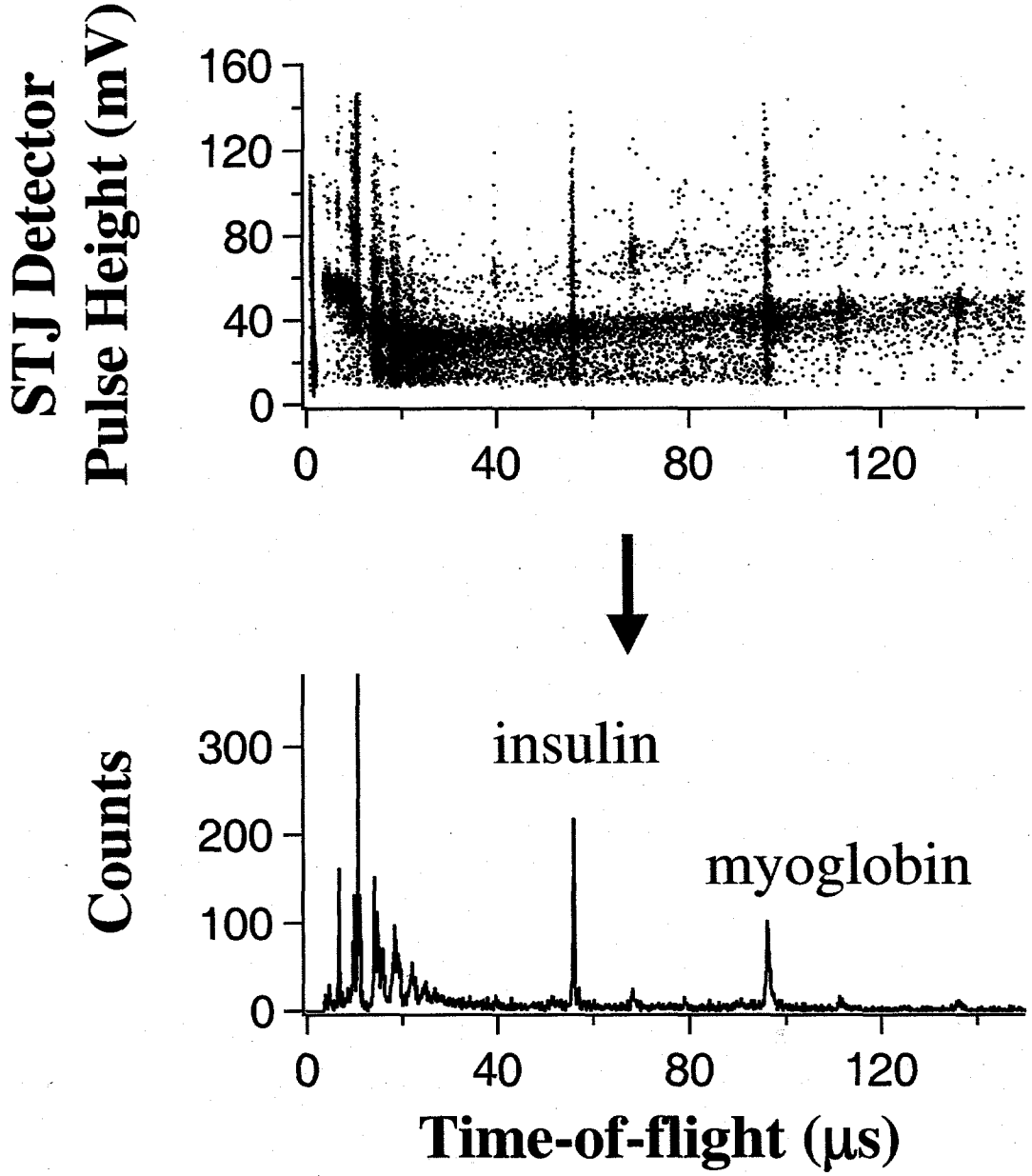
STJ Detector
Pulse Height (mV)
160
120
80
40
0
0
40
80
120
Counts
300
200
100
0
insulin
myoglobin
0
40
80
120
Time-of-flight (μs)

Fig.5

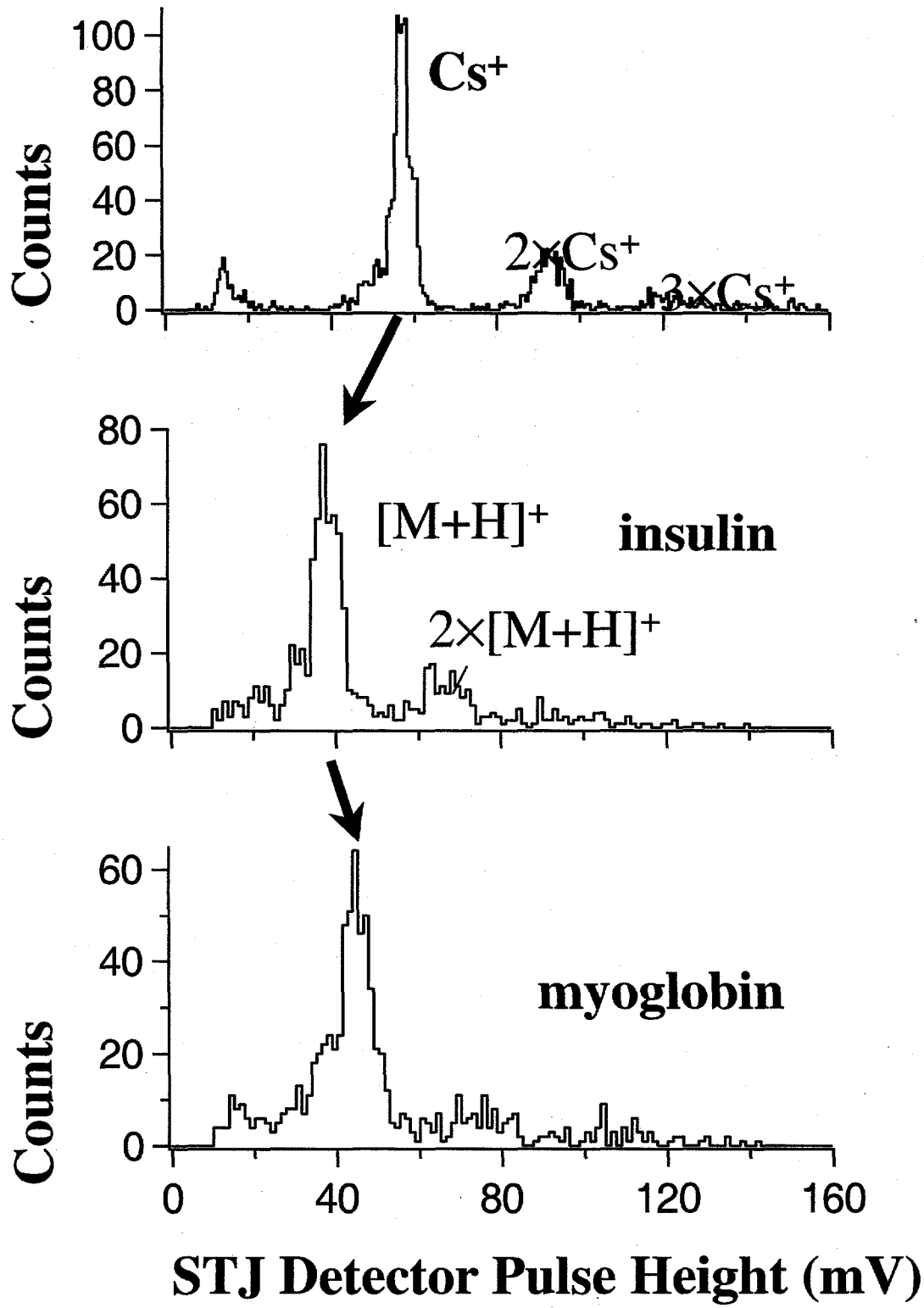
Counts
100
80
60
40
20
0
Cs+
2×Cs+
3×Cs+
Counts
80
60
40
20
0
[M+H]+
insulin
2×[M+H]+
Counts
60
40
20
0
myoglobin
0
40
80
120
160
STJ Detector Pulse Height (mV)

Fig.6

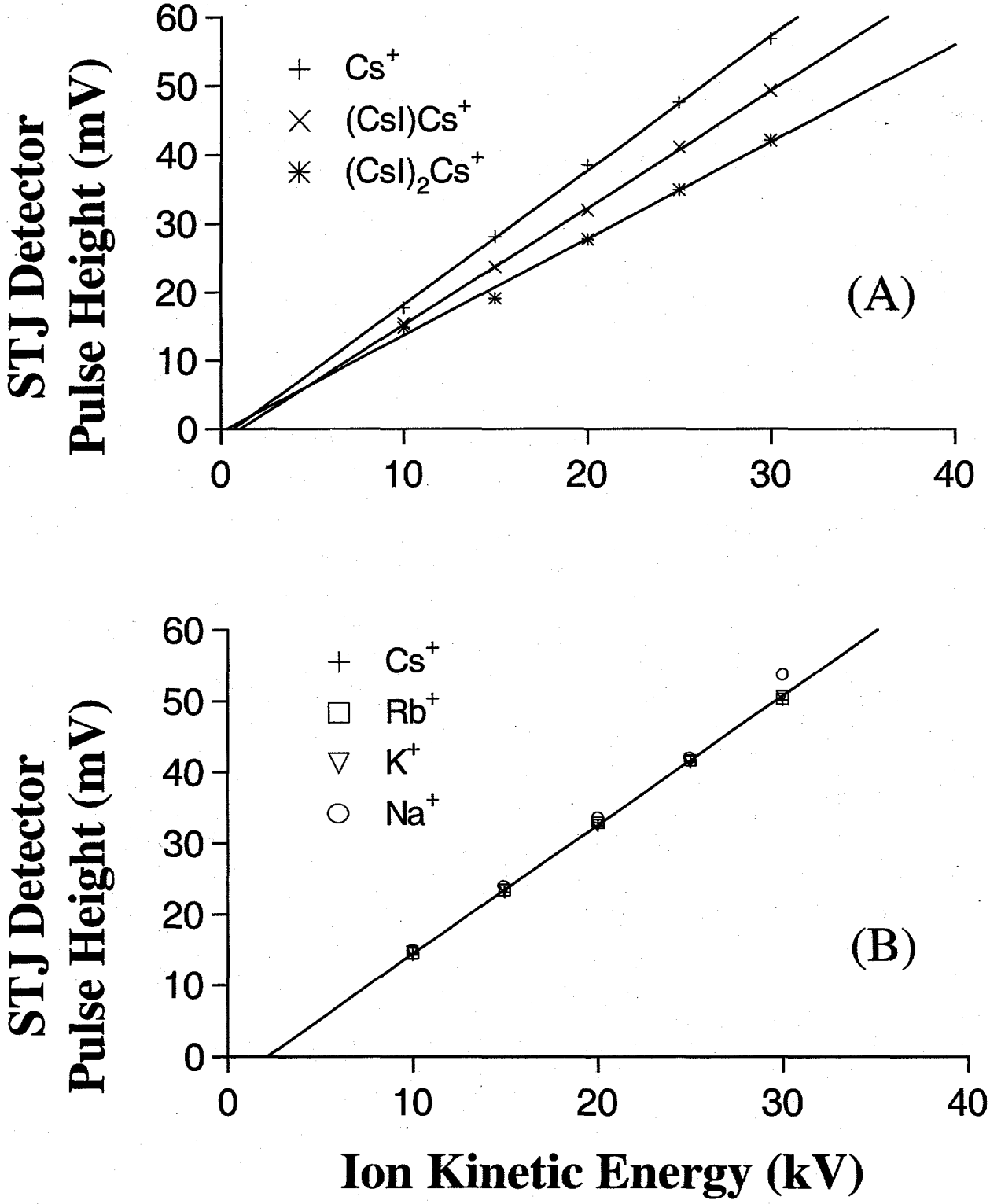
STJ Detector
Pulse Height (mV)
60
50
40
30
20
10
0
0
10
20
30
40
+ Cs+
× (CsI)Cs+
✳ (CsI)2Cs+
(A)
STJ Detector
Pulse Height (mV)
+ Cs+
□ Rb+
▽ K+
○ Na+
(B)
Ion Kinetic Energy (kV)

Fig.7

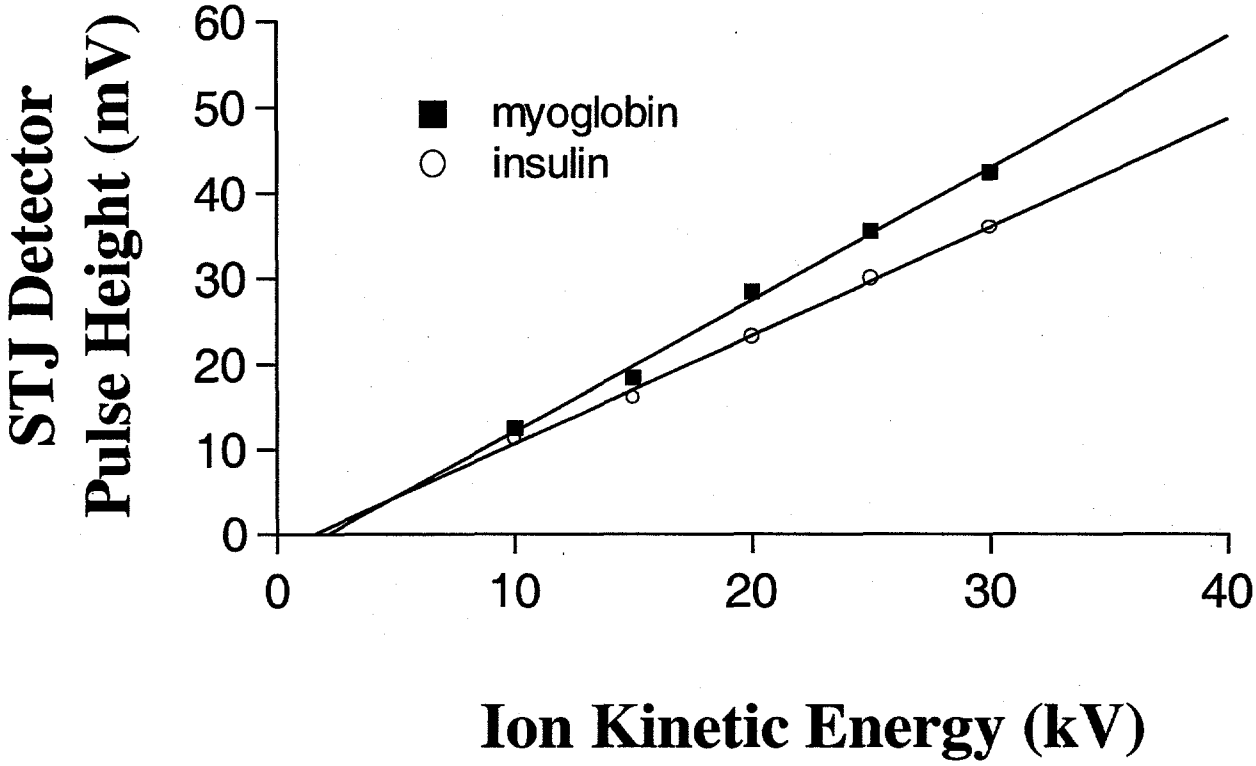
STJ Detector
Pulse Height (mV)
60
50
40
30
20
10
0
myoglobin
insulin
0
10
20
30
40
Ion Kinetic Energy (kV)

Fig.8

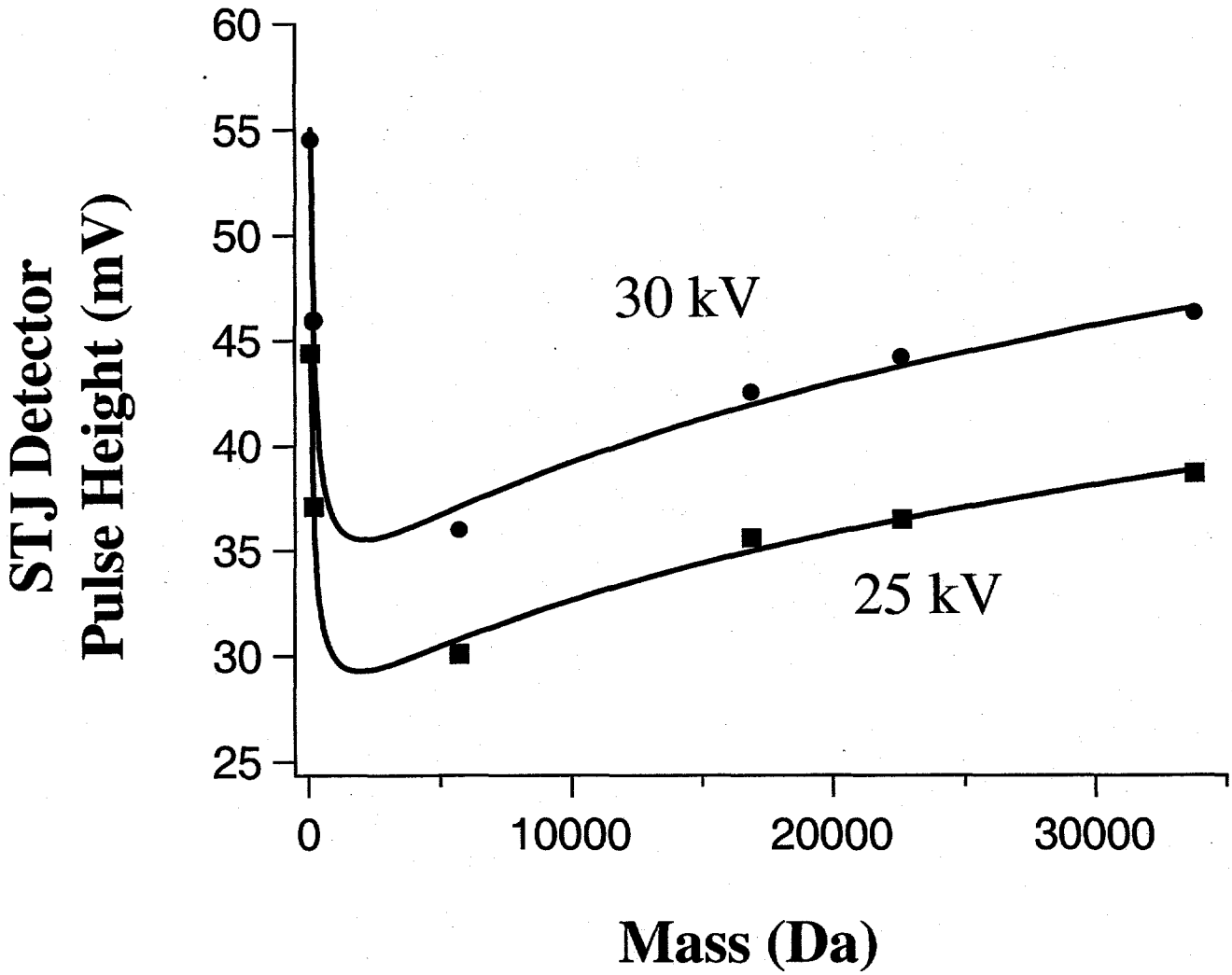
STJ Detector
Pulse Height (mV)
60
55
50
45
40
35
30
25
30 kV
25 kV
0
10000
20000
30000
Mass (Da)

Fig.9